A Generalized Framework for Microstructural Optimization using Neural Networks

Anonymous Author(s)
Affiliation
Address
email

Abstract

Microstructures, i.e., architected materials, are designed today, typically, by maximizing an objective, such as bulk modulus, subject to a volume constraint. However, in many applications, it is often more appropriate to impose constraints on other physical quantities of interest.

In this paper, we consider such generalized microstructural optimization problems where any of the microstructural quantities, namely, bulk, shear, Poisson ratio, or volume, can serve as the objective, while the remaining can serve as constraints. In particular, we propose here a neural-network (NN) framework to solve such problems. The framework relies on the classic density formulation of microstructural optimization, but the density field is represented through the NN's weights and biases.

The main characteristics of the proposed NN framework are: (1) it supports automatic differentiation, eliminating the need for manual sensitivity derivations, (2) smoothing filters are not required due to implicit filtering, (3) the framework can be easily extended to multiple-materials, and (4) a high-resolution microstructural topology can be recovered through a simple post-processing step. The framework is illustrated through a variety of microstructural optimization problems.

1 Introduction

Topology optimization is a computational strategy for distributing material within a design domain, to optimize performance. It is now a mature field with multitude of methods, including homogenization, density methods, level set, topological sensitivity and evolutionary [5, 32, 44, 11, 12, 41, 4, 18].

On the other hand, in *microstructural optimization*, one aims to find the optimal topology, within a representative unit cell, that maximizes a localized material property. Through microstructural design, one can customize various material behavior including bulk/shear modulus, Poisson's ratio, thermal expansion, elasticity tensor and other extremal properties[27, 20, 39, 45, 34, 31, 30].

There are many applications of microstructural optimization in engineering; for example, energy dissipation [3], fluid applications [16], thermal applications [50], phononic applications [35], medical implants [19], and so on. Further, with the advent of additive manufacturing, the fabrication of such microstructures is possible today. These microstructures, also referred to as *architected materials*, may be arranged in periodic arrays to *"exhibit previously unattainable combinations of material properties at the bulk scale."* [27]. In a typical microstructural optimization problem, one attempts to maximize a quantity of interest (such as bulk modulus), subject to a mass constraint (or equivalently,

Submitted to 36th Conference on Neural Information Processing Systems (NeurIPS 2022). Do not distribute.

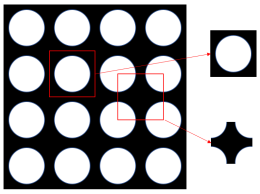

Figure 1: Locally periodic microstructures and unit cells.

volume-fraction constraint). However, in many applications, the desired mass is not known a priori. Therefore, instead of imposing an arbitrary mass constraint, we consider imposing constraints on other physical quantities. The main objective of this paper is to develop a framework for solving such generalized microstructural optimization problems.

Further, it has been observed [30] that the design of negative Poisson ratio (NPR) materials, using standard optimization techniques, can be particularly challenging. Either specialized methods need to be developed [48] or heuristic parameters must be used [43]. Here, we show that standard L-BFGS optimization can be used for the robust design of NPR materials.

The remainder of this paper is organized as follows. First, the critical concept of homogenization is briefly reviewed in Section 2.1. Then, the current methods of microstructural optimization are reviewed in Section 2.2, with an emphasis on the classic density-based formulation. Then, in Section 3.1, a generalized microstructural optimization problem. To solve such a class of problems, we introduce a neural-network (NN) framework in Section 3.2 where the density field is represented through the weights associated with the NN. This allows for automatic sensitivity computation which is essential for solving generalized problems. In Section 3.3 the methodology to solve such generalized problems is discussed followed by the proposed algorithm in Section A.1. Numerical examples are presented in Section 4. Finally, conclusions and open issues are discussed in Section 5.

2 Background

2.1 Homogenization

In microstructural design, a common hypothesis is that the microstructure is locally periodic, and there is scale separation. For example, Figure illustrates locally periodic microstructures and two representative unit cells.

Given a unit cell (microstructure) in 2D, a forward problem is to find its homogenized elasticity 3×3 matrix $\boldsymbol{C}^H$. The theory of homogenization is well developed, for example, see [47, 18]. A typical numerical strategy [1] for computing $\boldsymbol{C}^H$ is to impose three independent periodic boundary conditions (in 2D), and solve the resulting finite element problems; see Figure 2. The stresses and strains from the three problems are then used to compute $\boldsymbol{C}^H$ as described in [1].

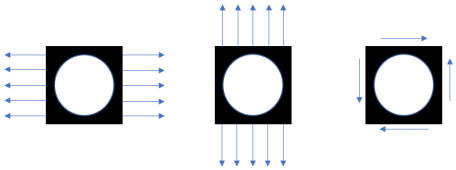

Figure 2: Extracting the elasticity tensor.

Next, assuming isotropic, plane stress behavior[36], various quantities of interest, namely, bulk modulus (K), shear modulus (G) and Poisson ratio (ν) can be extracted from $\boldsymbol{C}^H$ as follows:

$$K = (C^H_{1,1} + C^H_{2,2} + C^H_{1,2} + C^H_{2,1})/4 \tag{1a}$$

$$G = C^H_{3,3} \tag{1b}$$

$$\nu = (C^H_{2,1} + C^H_{1,2})/(C^H_{1,1} + C^H_{2,2}) \tag{1c}$$

2.2 Microstructural Optimization Methods

The inverse problem is to arrive at an optimal topology that maximizes or minimizes one of these quantities of interest. There are several methods available today for optimizing microstructures; see, for example, [27, 14, 39, 37, 21, 17].

In the popular density-based methods, one defines a pseudo-density $\rho_e \in (0, 1]$ over the underlying finite element mesh. Then the microstructural optimization problem, of say, maximizing the bulk modulus, subject to a mass constraint (we prefer here a mass constraint over a volume constraint since this generalizes more easily to multiple materials), may be posed as follows:

$$\underset{\boldsymbol{\rho}}{\text{minimize}} \quad -K(\boldsymbol{\rho}) \tag{2a}$$

$$\text{subject to} \quad \mathbf{K}(\boldsymbol{\rho})\boldsymbol{u}^i = \boldsymbol{f}^i, i = 1, 2, 3 \tag{2b}$$

$$\sum_e \rho_e v_e \lambda_e = \hat{m} \tag{2c}$$

$$0 < \rho_e \leq 1 \tag{2d}$$

where $\mathbf{K}$ is the stiffness matrix, $\boldsymbol{u}^i$ and $\boldsymbol{f}^i$ are the displacement vector and the external force vector for the three problems in Figure 2, v_e is the volume of the finite element, λ_e is the physical density of the base material, and $\hat{m}$ is the mass constraint. In addition, the solid isotropic material with penalization (SIMP) penalization model is employed to link the density variables to the base material

$$E(\rho_e) = E_{min} + E\rho_e^p \tag{3}$$

The field can now be optimized using, for example, optimality criteria [6] or MMA [38], resulting in the desired microstructural topology; see [43], for example. Similar problems can be posed, for example, to minimize the Poisson ratio, subject to a mass constraint.

3 Proposed Framework

3.1 Generalized Microstructural Problems

As stated earlier, in many applications, the mass constraint $\hat{m}$ (see Equation 2c) is not known a priori. Instead, it may be more advantageous to impose constraints on physical quantities. In this paper, we consider such generalized microstructural optimization problems of the form:

$$\underset{\boldsymbol{\rho}}{\text{minimize}} \quad \phi(\boldsymbol{C}^H(\boldsymbol{\rho})) \tag{4a}$$

$$\text{subject to} \quad \boldsymbol{K}(\boldsymbol{\rho})\boldsymbol{u}^i = \boldsymbol{f}^i, i = 1, 2, 3 \tag{4b}$$

$$h_j(\boldsymbol{\rho}) = 0, j = 1, 2, ... \tag{4c}$$

$$0 < \boldsymbol{\rho} \leq 1 \tag{4d}$$

where the objective $\phi(\boldsymbol{C}^H)$ represents one of the following: the bulk modulus (K), shear modulus (G), Poisson ratio (ν), that depend on the density via the elasticity matrix, or mass (m) that depends directly on the density, and h_j are equality constraints involving these quantities.

For example, the problem of maximizing the bulk modulus subject to a Poisson ratio constraint may be posed as:

$$\underset{\boldsymbol{\rho}}{\text{minimize}} \quad -K(\boldsymbol{\rho}) \tag{5a}$$

$$\text{subject to} \quad \boldsymbol{K}(\boldsymbol{\rho})\boldsymbol{u}^i = \boldsymbol{f}^i, i = 1, 2, 3 \tag{5b}$$

$$\nu(\boldsymbol{\rho})/\hat{\nu} - 1 = 0 \tag{5c}$$

$$0 < \boldsymbol{\rho} \leq 1 \tag{5d}$$

where $\hat{\nu}$ is the desired Poisson ratio. Similarly, the problem of minimizing the mass subject to constraints on the bulk modulus and Poisson ratio may be posed as:

$$\underset{\boldsymbol{\rho}}{\text{minimize}} \quad m(\boldsymbol{\rho}) \tag{6a}$$

$$\text{subject to} \quad \boldsymbol{K}(\boldsymbol{\rho})\boldsymbol{u}^i = \boldsymbol{f}^i, i = 1, 2, 3 \tag{6b}$$

$$K(\boldsymbol{\rho})/\hat{K} - 1 = 0 \tag{6c}$$

$$\nu(\boldsymbol{\rho})/\hat{\nu} - 1 = 0 \tag{6d}$$

$$0 < \boldsymbol{\rho} \leq 1 \tag{6e}$$

where $\hat{K}$ is the desired bulk modulus, and $\hat{\nu}$ is the desired Poisson ratio. In the remainder of this paper, we will consider solving such problems.

3.2 Representing Density using Neural Networks

One of the challenges in solving such generalized problems is computing the sensitivities of the objective and constraints. Manual derivation can be cumbersome and error-prone, especially when the problem is recast within the context of augmented Lagrangian formulation (see Section 3.3). We, therefore, propose here a neural-network (NN) framework that supports automatic sensitivity computation for gradient-based optimization [8]. The framework not only eliminates the burden of manual sensitivity calculations, it offers other computational advantages as discussed in the remainder of the paper.

In particular, we employ a simple fully-connected feed-forward neural network [7]. The input to the network are points (x, y) within the domain; the NN has a series of hidden layers associated with activation functions [15], [24]. The output is the density ρ at that point; see Figure 3. Observe that the final layer is a SoftMax activation function [7] that ensures that the density lies between 0 and 1. The density will depend on the weights and bias, i.e., they serve as the design variables $\boldsymbol{w}$.

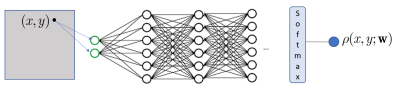

Figure 3: Neural network architecture for representing the density field.

Thus, we can now repose the generalized problem as:

$$\underset{\boldsymbol{w}}{\text{minimize}} \quad \phi(\boldsymbol{C}^H(\boldsymbol{w})) \tag{7a}$$

$$\text{subject to} \quad \boldsymbol{K}(\boldsymbol{w})\boldsymbol{u}^i = \boldsymbol{f}^i, i = 1, 2, 3 \tag{7b}$$

$$h_j(\boldsymbol{w}) = 0, j = 1, 2, ...n \tag{7c}$$

Observe that an explicit (bound) constraint on the density field is not needed since it is automatically satisfied by the Softmax function.

To generalize the above framework to multiple materials, the output of the NN is increased to $(M+1)$ variables, where M is the number of non-void materials; see Figure 4. No other change is needed in the framework, i.e., one can use exactly the same number of design variables $\boldsymbol{w}$. Further, due to the nature of Softmax function, the partition of unity condition:

$$\sum_{m=0}^{M} \rho_m = 1 \tag{8}$$

is automatically satisfied, i.e., the sum of all densities is guaranteed to be unity. Finally, the SIMP material model in Equation 3 is generalized to multiple materials as follows:

$$E(\rho) = E_{min} + \sum_{m=0}^{M} E_m \rho_m^p \tag{9}$$

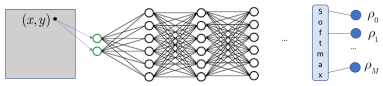

Figure 4: Neural network architecture for representing multiple materials.

3.3 Augmented Lagrangian

To solve both the single and multi-material problems, we will use the augmented Lagrangian method [26], i.e., let

$$L(\boldsymbol{w}) = \phi + \sum_{j=1,2\ldots}^{n} \alpha_j h_j^2 + \sum_{j=1,2\ldots}^{n} \mu_j h_j \tag{10}$$

where the penalty parameters α_j and Lagrange multipliers μ_j are updated through iterations. First, starting with a small value for α_j and a zero value for μ_j the augmented Lagrangian is minimized using the popular L-BFGS method [26]. Then, the coefficients α and μ are updated as follows (see Section 4):

$$\alpha_j{}^{(k+1)} = \alpha_j{}^{(k)} + \Delta\alpha \tag{11a}$$

$$\mu_j{}^{(k+1)} = \mu_j{}^{(k)} + 2\alpha_j{}^{(k+1)} h_j^{(k)} \tag{11b}$$

The optimization is repeated until convergence. For termination, we consider two quantities

$$\epsilon_\phi = \mid (\phi^{(k+1)} - \phi^{(k)})/\phi^{(k+1)} \mid \tag{12}$$

and

$$\epsilon_h = \sum_{j=1,2\ldots}^{n} \mid h_j \mid \tag{13}$$

The algorithm terminates when both quantities are less than a prescribed value (see Section 4 for details). The overall framework is illustrated in Figure 5.

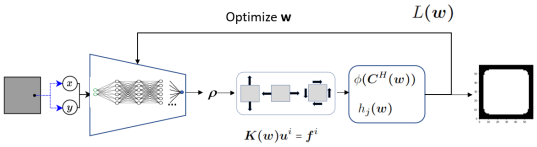

Figure 5: The optimization framework.

3.4 Automatic Differentiation

Since L-BFGS is a gradient-based optimizer, it requires sensitivities, i.e., derivative of the loss function with respect to the design variables (weights of the NN). In the present framework, all computations including FEA are captured using PyTorch (that supports automatic differentiation) as illustrated in fig. 6. Thus, not only can we compute the spatial gradients of the density field, one can also compute the sensitivities of the loss function with respect to the weights in an automated fashion as illustrated.

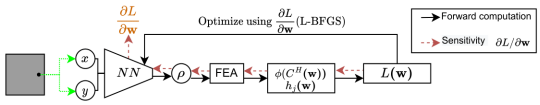

Figure 6: Automatic differentiation provides sensitivities for L-BFGS.

4 Numerical examples

In this section, we conduct several numerical experiments to illustrate the proposed algorithm (refer Appendix for algorithm). The implementation is in Python, within the PyTorch environment. All experiments were conducted on an Intel i9-11900K @ 3.50GHz GHz, equipped with 32 GB of RAM. The default parameters are listed in Table 1. We use the popular SIMP continuation scheme [29] for the material model. For the default NN configuration of 5 layers and 30 neurons per layer, the number of design variables $\boldsymbol{w}$ (weight and bias) is 3872.

Parameter	Description and default value
E, ν	For base material: $E = 1$, $\nu = 0.3$; for void: $E = 0.001$, $\nu = 0.3$
λ(mass density)	For base material: $\lambda = 1$; for void: $\lambda = 0$
NN	Neural network: 5 layers and 30 neurons per layer, with Swish functions
α, μ	Lagrangian parameters: $\alpha_0 = 1$, $\Delta\alpha = 5$ and $\mu_0 = 0$
p	SIMP continuation parameters: $p_0 = 2$, $\Delta p = 0.5$, $p_{max} = 10$
n_x,n_y	Mesh elements: $n_x = 60$, $n_y = 60$
$\hat{\epsilon}_\phi$, $\hat{\epsilon}_h$	Convergence criteria for objective and constraints: $\hat{\epsilon}_\phi$ = $\hat{\epsilon}_h$ = 0.025

Table 1: Default simulation parameters.

The default initial topology is a square block as illustrated in Figure 7.

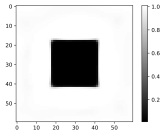

Figure 7: Default initial topology.

Through the experiments, we investigate the following:

1. *Validation*: First, we consider classic mass constrained optimization of bulk modulus, shear modulus, and Poisson ratio, and compare some of the computed values against well-established theoretical results.
2. *Convergence*: The typical convergence of the algorithm is then illustrated.
3. *Initial Topology*: Next, we consider initial topologies different from the one in Figure 7 and optimize for maximum bulk modulus.(Appendix)
4. *Impact of NN Configuration*: We then vary the NN size and consider its impact on Poisson ratio minimization. (Appendix)
5. *Impact of Mesh Size*: We repeat the above experiment but vary the mesh size instead of the NN size.(Appendix)
6. *Generalized Problems*: We then consider several generalized microstructural problems.
7. *High Resolution Sampling*: We then discuss the idea of high-resolution sampling that the proposed framework supports.(Appendix)
8. *Evaluation of Poisson Ratio*: For designs with negative Poisson ratio, we compare the predicted homogenized Poisson ratio against those predicted through a full-scale analysis using ANSYS.(Appendix)
9. *Multi-Material Design*: Finally, we present results for multiple materials.(Appendix)

4.1 Validation

First, we consider the classic problem of bulk modulus maximization subject to a mass-fraction constraint of 0.3. The resulting topology, computed in 47 seconds, is illustrated in Figure 8a. Similarly, Figure 8b illustrates a microstructure with maximal shear modulus for the same mass constraint, computed in 53 seconds. Finally, Figure 8c illustrates the microstructure when the Poisson ratio is minimized for the same mass constraint, computed in 55 seconds.

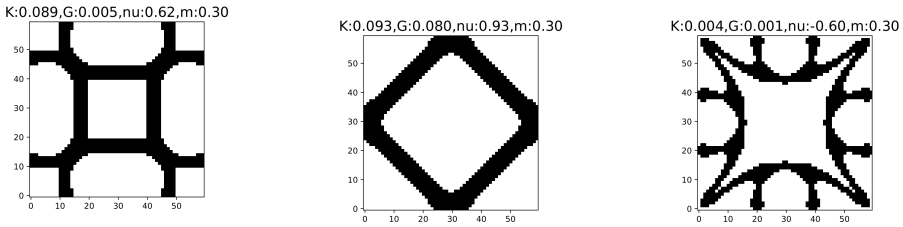

(a) Bulk modulus. (b) Shear modulus. (c) Poisson ratio.

Figure 8: Classic microstructural optimization problems.

Table 2 compares the computed bulk modulus for various mass fractions, against the Hashin-Shtrikman upper bound.

$\hat{m}$	K^*	K_{HS}
0.1	0.020	0.0282
0.3	0.092	0.099
0.5	0.18	0.20
0.7	0.34	0.35

Table 2: Computed bulk modulus vs. HS upper bound.

4.2 Convergence

Recall that the error in the objective ϵ_ϕ and error in the constraints ϵ_g, defined in Equation 12 and Equation 13 respectively, are computed at the end of every L-BFGS iteration. The algorithm terminates when $\epsilon_\phi < \hat{\epsilon}_\phi$ *and* $\epsilon_g < \hat{\epsilon}_g$ specified in Table 1. Figure 9a illustrates the objective error ϵ_ϕ and the constraint error ϵ_g for bulk modulus maximization, while Figure 9b illustrates the two errors for Poisson ratio minimization.

(a) Bulk modulus. (b) Poisson ratio.

Figure 9: Objective and constraint errors after every L-BFGS iteration.

In the experiments, we observed that 3 to 20 L-BFGS iterations are sufficient. Further, each L-BFGS iteration typically involves 2 to 10 inner iterations. The homogenized properties are recorded at the end of every inner iteration. Figure 10a illustrates these quantities for bulk modulus maximization, and Figure 10b illustrates these for Poisson ratio minimization. The spikes observed in the two figures correspond to the start of a new L-BFGS iteration when the penalty parameters are updated.

4.3 Generalized Problems

To illustrate the benefits of the proposed framework, we first used the MATLAB code published in [43] to minimize the Poisson ratio to a mass constraint of $\hat{m} = 0.5$. The algorithm did not terminate;

(a) Bulk modulus. (b) Poisson ratio.

Figure 10: Various homogenized quantities after every FE operation.

the final topology, after a maximum allowable 450 FE operations (15 seconds), is illustrated in Figure 11a; it exhibits the following characteristics $\nu = -0.23$, $K = 0.015$ and $G = 0.002$. Observe that the microstructure is weak in bulk and shear.

In the proposed framework, the bulk modulus was maximized subject to $\nu = -0.23$ and $\hat{m} = 0.5$, i.e., the constraints are consistent with the results obtained above. The resulting topology, after 420 FE operations (52 seconds), illustrated in Figure 11b exhibits the following characteristics $m = 0.5$, $\nu = -0.23$, $K = 0.027$ and $G = 0.012$. Thus the proposed framework increases the bulk modulus by a factor of about 2. For approximately the same number of finite element operations, the proposed framework is slower due to the overhead of automatic differentiation.

Next, the shear modulus was maximized subject to $\nu = -0.23$ and $\hat{m} = 0.5$. The resulting topology after 560 FE operations (91 seconds), illustrated in Figure 11c exhibits the following characteristics $m = 0.5$, $\nu = -0.23$, $K = 0.027$ and $G = 0.027$, i.e., the bulk and shear moduli increased by a factor of 10.

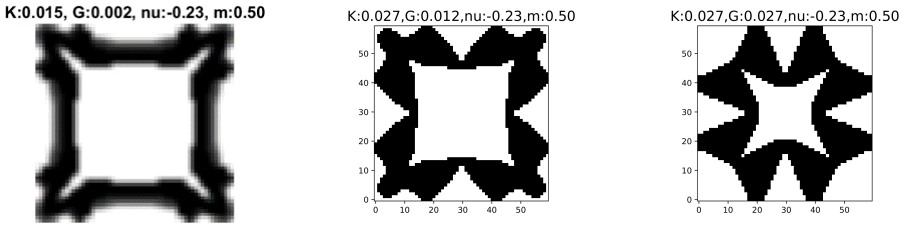

(a) Mass constrained. (b) Maximizing K. (c) Maximizing G.

Figure 11: Classic versus proposed framework.

One can also impose multiple physical constraints within the proposed framework. Consider the minimization of the mass, subject to bulk modulus and Poisson ratio constraints. Figure 12 illustrates three designs obtained for three different scenarios. The corresponding mass fractions are 0.34, 0.63, and 0.82. One can also target a specific elasticity matrix $\hat{\boldsymbol{C}}^H$. We consider a specific example from

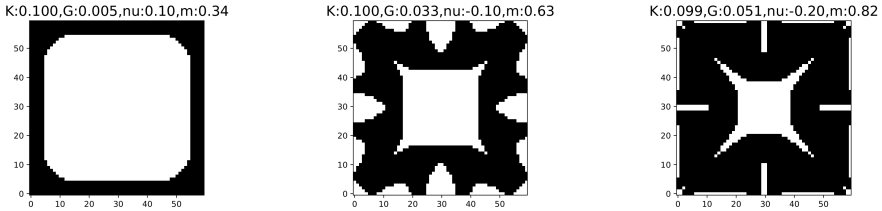

(a) $\hat{K} = 0.1$, $\hat{\nu} = 0.1$. (b) $\hat{K} = 0.1$, $\hat{\nu} = -0.1$. (c) $\hat{K} = 0.1$, $\hat{\nu} = -0.2$.

Figure 12: Minimizing mass with bulk modulus and Poisson ratio constraints.

[48]:

$$\hat{\boldsymbol{C}}^H = \begin{bmatrix} 0.13 & -0.03 & 0 \\ -0.03 & 0.13 & 0 \\ 0 & 0 & 0.015 \end{bmatrix} \tag{14}$$

Note that there may exist multiple solutions (with significantly different masses) with the same $\boldsymbol{C}^H$ [39]. Using our framework by imposing the target $\boldsymbol{C}^H$ and a target mass as constraints, one can obtain different designs; these are illustrated in Figure 13a and 13b, with mass target of 0.40 and 0.52, respectively. A solution, with a mass of 0.37 was reported in [48]; see Figure 13c.

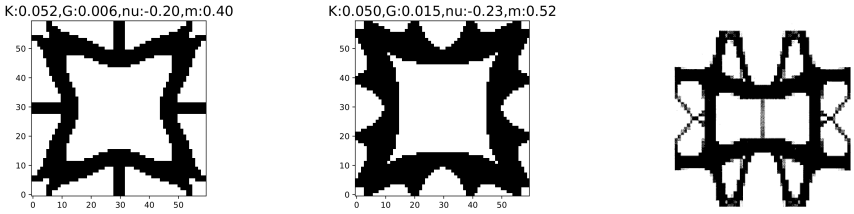

(a) m = 0.40 (b) m = 0.52 (c) m = 0.37 [48]

Figure 13: Designs obtained for a targeted $\hat{\boldsymbol{C}}^H$.

5 Conclusions

This paper presents a generalized neural-network-based framework for microstructural optimization where any of the microstructural quantities, namely, bulk, shear, Poisson ratio, volume or mass, can serve as the objective, while the remaining can be subject to constraints. Since the sensitivities are computed in automated fashion, one can avoid the error-prone task of manual derivations. This can be particularly useful, for example, when the material is non-linear. Further, we avoided heuristics for designing NPR materials. Instead we relied on standard L-BFGS optimization techniques. This supports repeatability and wider adaption of the framework as a powerful design tool. Due to the overhead cost of automatic differentiation (AD), the framework was found to be slower than, say, the MATLAB implementation presented in [43]. However, we believe the benefits of AD outweigh the computational costs. We also noted that the designs were sensitive to mesh discretization. Since this is not usually desirable in topology optimization, further investigation is needed to study the interplay between the neural network and mesh discretization.

There are several directions for future research: extension to multi-physics [10], 3D [2], geometric and material non-linearity [40], inclusion of stress constraints [9], multi-stable materials [46], and inclusion of feature size and manufacturing constraints [13, 22, 49] within the NN framework.

Acknowledgments

The authors would like to thank the support of the National Science Foundation through grant CMMI 1561899, and the U. S. Office of Naval Research under PANTHER award number N00014-21-1-2916 through Dr. Timothy Bentley.

Compliance with ethical standards

The authors declare that they have no conflict of interest.

Replication of Results

The Python code pertinent to this paper is available as supplementary material .

References

[1] E. Andreassen and C. S. Andreasen. How to determine composite material properties using numerical homogenization. *Computational Materials Science*, 83:488–495, 2014.

[2] Erik Andreassen, Boyan S Lazarov, and Ole Sigmund. Design of manufacturable 3d extremal elastic microstructure. *Mechanics of Materials*, 69(1):1–10, 2014.

[3] Alireza Asadpoure, Mazdak Tootkaboni, and Lorenzo Valdevit. Topology optimization of multiphase architected materials for energy dissipation. *Computer Methods in Applied Mechanics and Engineering*, 325:314–329, 2017.

[4] M. P. Bendsøe and N. Kikuchi. Generating optimal topologies in structural design using a homogenization method. *Computer Methods in Applied Mechanics and Engineering*, 71(2):197–224, nov 1988.

[5] M. P. Bendsøe and O. Sigmund. *Topology optimization*. Springer Berlin Heidelberg, 2004.

[6] M P Bendsoe and Ole. Sigmund. *Topology optimization: theory, methods, and applications*. Springer Berlin Heidelberg, 2 edition, 2003.

[7] Christopher M Bishop. *Pattern recognition and machine learning*. springer, 2006.

[8] Aaditya Chandrasekhar, Saketh Sridhara, and Krishnan Suresh. Auto: a framework for automatic differentiation in topology optimization. *Structural and Multidisciplinary Optimization*, 64(6):4355–4365, Dec 2021.

[9] Maxime Collet, Lise Noël, Matteo Bruggi, and Pierre Duysinx. Topology optimization for microstructural design under stress constraints. *Structural and Multidisciplinary Optimization*, 58(6):2677–2695, 2018.

[10] Sourav Das and Alok Sutradhar. Multi-physics topology optimization of functionally graded controllable porous structures: Application to heat dissipating problems. *Materials & Design*, 193:108775, 2020.

[11] Shiguang Deng and Krishnan Suresh. Multi-constrained topology optimization via the topological sensitivity. *Structural and Multidisciplinary Optimization*, 51(5):987–1001, 2015.

[12] Shiguang Deng and Krishnan Suresh. Stress constrained thermo-elastic topology optimization with varying temperature fields via augmented topological sensitivity based level-set. *Structural and Multidisciplinary Optimization*, 56(6):1413–1427, 2017.

[13] Zongliang Du, Xiao-Yi Zhou, Renato Picelli, and H Alicia Kim. Connecting microstructures for multiscale topology optimization with connectivity index constraints. *Journal of Mechanical Design*, 140(11):111417, 2018.

[14] Jie Gao, Hao Li, Zhen Luo, Liang Gao, and Peigen Li. Topology optimization of microstructured materials featured with the specific mechanical properties. *International Journal of Computational Methods*, 17(03):1850144, 2020.

[15] Ian Goodfellow, Yoshua Bengio, and Aaron Courville. *Deep Learning*. MIT Press, 2016.

[16] James K Guest and Jean H Prévost. Optimizing multifunctional materials: design of microstructures for maximized stiffness and fluid permeability. *International Journal of Solids and Structures*, 43(22-23):7028–7047, 2006.

[17] Kai Guo and Markus J Buehler. A semi-supervised approach to architected materials design using graph neural networks. *Extreme Mechanics Letters*, 41:101029, 2020.

[18] B. Hassani and E. Hinton. A review of homogenization and topology optimization I - Homogenization theory for media with periodic structure. *Computers and Structures*, 69(6):707–717, 1998.

[19] Meng-Ting Hsieh, Matthew R Begley, and Lorenzo Valdevit. Architected implant designs for long bones: Advantages of minimal surface-based topologies. *Materials & Design*, 207:109838, 2021.

[20] X. Huang, A. Radman, and Y. M. Xie. Topological design of microstructures of cellular materials for maximum bulk or shear modulus. *Computational Materials Science*, 50(6):1861–1870, 2011.

[21] Hunter T Kollmann, Diab W Abueidda, Seid Koric, Erman Guleryuz, and Nahil A Sobh. Deep learning for topology optimization of 2d metamaterials. *Materials & Design*, 196:109098, 2020.

[22] B. S. Lazarov, F. Wang, and O. Sigmund. Length scale and manufacturability in density-based topology optimization. *Archive of Applied Mechanics*, 86(1-2):189–218, 2016.

[23] Chenxi Lu, Mengting Hsieh, Zhifeng Huang, Chi Zhang, Yaojun Lin, Qiang Shen, Fei Chen, and Lianmeng Zhang. Architectural design and additive manufacturing of mechanical metamaterials: A review. *Engineering*, 2022.

[24] Lu Lu, Yeonjong Shin, Yanhui Su, and George Em Karniadakis. Dying relu and initialization: Theory and numerical examples. *arXiv preprint arXiv:1903.06733*, 2019.

[25] Erdogan Madenci and Ibrahim Guven. *The finite element method and applications in engineering using ANSYS®*. Springer, 2015.

[26] Jorge Nocedal and Stephen Wright. *Numerical optimization*. Springer Science & Business Media, 2006.

[27] M. Osanov and J. K. Guest. Topology optimization for architected materials design. *Annual Review of Materials Research*, 46(1):211–233, 2016.

[28] Xiaoping Qian. Topology optimization in b-spline space. *Computer Methods in Applied Mechanics and Engineering*, 265:15–35, 2013.

[29] S. Rojas-Labanda and M. Stolpe. Automatic penalty continuation in structural topology optimization. *Structural and Multidisciplinary Optimization*, 52(6):1205–1221, 2015.

[30] O. Sigmund. Materials with prescribed constitutive parameters: An inverse homogenization problem. *International Journal of Solids and Structures*, 31(17):2313–2329, 1994.

[31] O. Sigmund. New class of extremal composites. *Journal of the Mechanics and Physics of Solids*, 48(2):397–428, 2000.

[32] O. Sigmund and K. Maute. Topology optimization approaches: A comparative review. *Structural and Multidisciplinary Optimization*, 48(6):1031–1055, 2013.

[33] O. Sigmund and J. Petersson. Numerical instabilities in topology optimization: A survey on procedures dealing with checkerboards, mesh-dependencies and local minima. *Structural Optimization*, 16(1):68–75, 1998.

[34] O. Sigmund and S. Torquato. Design of materials with extreme thermal expansion using a three-phase topology optimization method. Technical Report 6, 1997.

[35] Ole Sigmund and Jakob Søndergaard Jensen. Systematic design of phononic band–gap materials and structures by topology optimization. *Philosophical Transactions of the Royal Society of London. Series A: Mathematical, Physical and Engineering Sciences*, 361(1806):1001–1019, 2003.

[36] Ole Sigmund and Salvatore Torquato. Design of smart composite materials using topology optimization. *Smart Materials and Structures*, 8(3):365, 1999.

[37] K. Suresh. Efficient microstructural design for additive manufacturing. In *ASME 2014 International Design Engineering Technical Conferences and Computers and Information in Engineering Conference*, 2014.

[38] Krister Svanberg. The method of moving asymptotes—a new method for structural optimization. *International journal for numerical methods in engineering*, 24(2):359–373, 1987.

[39] P. Vogiatzis, S. Chen, X. Wang, T. Li, and L. Wang. Topology optimization of multi-material negative Poisson's ratio metamaterials using a reconciled level set method. *CAD Computer Aided Design*, 83:15–32, 2017.

[40] Mathias Wallin and Daniel A Tortorelli. Nonlinear homogenization for topology optimization. *Mechanics of Materials*, 145:103324, 2020.

[41] M.Y. Wang, X. Wang, and D. Guo. A level set method for structural topology optimization. *Computer Methods in Applied Mechanics and Engineering*, 192(1-2):227–246, jan 2003.

[42] Jinglai Wu, Zhen Luo, Hao Li, and Nong Zhang. Level-set topology optimization for mechanical metamaterials under hybrid uncertainties. *Computer Methods in Applied Mechanics and Engineering*, 319:414–441, 2017.

[43] Liang Xia and Piotr Breitkopf. Design of materials using topology optimization and energy-based homogenization approach in matlab. *Structural and multidisciplinary optimization*, 52(6):1229–1241, 2015.

[44] Y. M. Xie and G. P. Steven. A simple evolutionary procedure for structural optimization. *Computers and Structures*, 49(5):885–896, dec 1993.

[45] Y. M. Xie, X. Yang, J. Shen, X. Yan, A. Ghaedizadeh, J. Rong, X. Huang, and S. Zhou. Designing orthotropic materials for negative or zero compressibility. *International Journal of Solids and Structures*, 51(23-24):4038–4051, 2014.

[46] Hang Yang and Li Ma. 1d to 3d multi-stable architected materials with zero poisson's ratio and controllable thermal expansion. *Materials & Design*, 188:108430, 2020.

[47] Hua Yang, Bilen Emek Abali, Dmitry Timofeev, and Wolfgang H Müller. Determination of metamaterial parameters by means of a homogenization approach based on asymptotic analysis. *Continuum mechanics and thermodynamics*, 32(5):1251–1270, 2020.

[48] Luzhong Yin and Wei Yang. Optimality criteria method for topology optimization under multiple constraints. *Computers & Structures*, 79(20-21):1839–1850, 2001.

[49] Jonas Zehnder, Yue Li, Stelian Coros, and Bernhard Thomaszewski. Ntopo: Mesh-free topology optimization using implicit neural representations. *Advances in Neural Information Processing Systems*, 34:10368–10381, 2021.

[50] Shiwei Zhou and Qing Li. Computational design of multi-phase microstructural materials for extremal conductivity. *Computational Materials Science*, 43(3):549–564, 2008.

Checklist

1. For all authors...
   (a) Do the main claims made in the abstract and introduction accurately reflect the paper's contributions and scope? [Yes]
   (b) Did you describe the limitations of your work? [Yes]
   (c) Did you discuss any potential negative societal impacts of your work? [N/A]
   (d) Have you read the ethics review guidelines and ensured that your paper conforms to them? [Yes]
2. If you are including theoretical results...
   (a) Did you state the full set of assumptions of all theoretical results? [Yes]
   (b) Did you include complete proofs of all theoretical results? [Yes]
3. If you ran experiments...
   (a) Did you include the code, data, and instructions needed to reproduce the main experimental results (either in the supplemental material or as a URL)? [Yes]
   (b) Did you specify all the training details (e.g., data splits, hyperparameters, how they were chosen)? [Yes]
   (c) Did you report error bars (e.g., with respect to the random seed after running experiments multiple times)? [Yes]
   (d) Did you include the total amount of compute and the type of resources used (e.g., type of GPUs, internal cluster, or cloud provider)? [Yes]
4. If you are using existing assets (e.g., code, data, models) or curating/releasing new assets...

(a) If your work uses existing assets, did you cite the creators? [N/A]
(b) Did you mention the license of the assets? [N/A]
(c) Did you include any new assets either in the supplemental material or as a URL? [N/A]

(d) Did you discuss whether and how consent was obtained from people whose data you're using/curating? [N/A]
(e) Did you discuss whether the data you are using/curating contains personally identifiable information or offensive content? [N/A]

5. If you used crowdsourcing or conducted research with human subjects...
   (a) Did you include the full text of instructions given to participants and screenshots, if applicable? [N/A]
   (b) Did you describe any potential participant risks, with links to Institutional Review Board (IRB) approvals, if applicable? [N/A]
   (c) Did you include the estimated hourly wage paid to participants and the total amount spent on participant compensation? [N/A]

A Appendix

A.1 Algorithm

The algorithm for the proposed framework is described in algorithm 1. First, the target design objective ϕ and the set of equality constraints h_j are specified along with an initial topology. Note that defining an initial topology is equivalent to initializing the neural network (NN). Thus the NN is initialized such that the density output matches the desired initial topology. Next, the domain is discretized into finite elements and the element centers serve as input to the neural network, which returns the elemental densities $\boldsymbol{\rho}$ as discussed in section 3.2. Homogenization is performed which predicts the homogenized structural response from the elemental densities as per section 2.1. Based on the results from homogenization, the objective ϕ eq. (7a) and the constraints h_j eq. (7c) are evaluated. Next, the loss function L is computed using eq. (10), and the gradient of the loss function with respect to the neural network weights (∇L) is computed through automatic differentiation. The NN is then trained using PyTorch's L-BFGS optimizer as described in section 3.3, which requires the update of Lagrangian parameters α, μ. The training procedure continues until the convergence criteria are met. The globally-defined activation functions, used in representing the density field, provide for implicit filtering. This is analogous to implicit filtering supported by the B-spline representation of the density field [28].

Algorithm 1 Microstructural TO using NN

procedure MICROTOUNN(Ω_0, ϕ, ...) ▷ Inputs
  $\Omega^{init} \rightarrow \boldsymbol{w}$ ▷ Initialize NN weights
  $\Omega^0 \rightarrow \Omega^0_h$ ▷ Domain discretization
  $\boldsymbol{x} = \{x_e, y_e\}_{e \in \Omega^0_h}$ ▷ elem centers; NN input
  k = 0; $\alpha_i = \alpha_0$; $\mu_i = 0 \; \forall i$ ▷ Initialization (section 3.3)
  repeat ▷ Optimization (Training)
    $NN(\boldsymbol{x}; \boldsymbol{w}) \rightarrow \boldsymbol{\rho}$ ▷ Fwd prop NN
    $\boldsymbol{\rho} \rightarrow \boldsymbol{C}^H$ ▷ Homogenization (section 2.1)
    $\boldsymbol{C}^H \rightarrow \phi$ ▷ Compute design objective eq. (7a)
    $\{\boldsymbol{C}^H, \boldsymbol{\rho}\} \rightarrow h_j$ ▷ Compute constraints eq. (7c)
    $\{\phi, h, \alpha_i, \mu_i\} \rightarrow L$ ▷ Loss from Equation (10)
    $AD(L \leftarrow \boldsymbol{w}) \rightarrow \nabla L$ ▷ Auto diff for sensitivity
    $\boldsymbol{w} + \Delta \boldsymbol{w}(\nabla L) \rightarrow \boldsymbol{w}$ ▷ L-BFGS step
    k + +
    Update α_i, μ_i ▷ Aug-Lag terms eq. (11a), eq. (11b)
  until $\Delta\phi < \hat{\epsilon}_\phi$ and $\Delta h < \hat{\epsilon}_h$ and $k < k_{max}$ ▷ convg. criteria
  return $\boldsymbol{w}$
end procedure

A.2 Impact of Initial Topology

Next, we consider initial designs different from Figure 7 and study their impact on the optimal topology, with all other parameters are kept constant at default values. Specifically, we revisit the problem of maximizing the bulk modulus, subject to a mass-fraction constraint of 0.3.

For the initial topology of a circular hole in Figure 14a, the final topology is illustrated in Figure 14b. Similarly, with the initial topology of four circular holes in Figure 15a, the final topology, for the

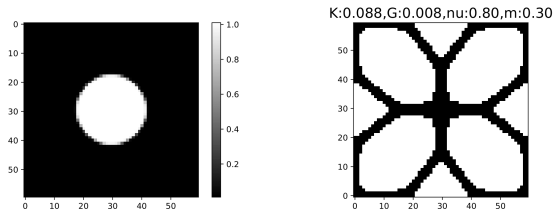

(a) Initial topology. (b) Final topology.

Figure 14: Maximizing bulk modulus with mass constraint.

same problem is illustrated in Figure 15b, with $K^* = 0.089$.

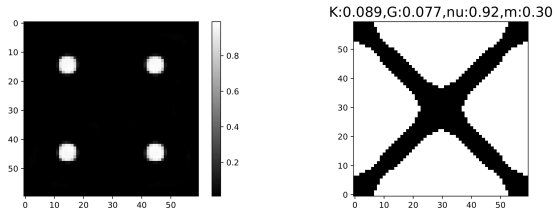

(a) Initial topology. (b) Final topology.

Figure 15: Maximizing bulk modulus with mass constraint.

Although the designs are different, the final bulk moduli are comparable. Thus, one can potentially discover different designs by changing the initial design.

A.3 Impact of NN Size

We now vary the neural-network size and minimize the Poisson ratio, subject to a mass-fraction constraint of 0.3 (with default parameters). Figure 16 illustrates various designs obtained for different NN configurations. The final Poisson ratio ν^* for the three cases are -0.60, -0.57 and -0.82 respectively. The number of design variables are 272, 1782 and 18,602 respectively. We observe that as the number of design variables is increased, the algorithm tends to generate more complex designs. But, we did not observe any pattern between the NN size and the final objective achieved. One can however observe single-node connections in some of the designs; this has been observed in NPR designs by other researchers as well [30]; dilation methods such as the ones proposed in[2] need to be explored to address this issue.

A.4 Impact of Mesh Size

Next, we vary the mesh size and minimize the Poisson ratio, subject to a mass constraint of 0.3 (with all other parameters at default). Figure 17 illustrates the designs obtained for different mesh sizes. The final Poisson ratio ν^* for the three cases are -0.57, -0.60 and -0.86 respectively. We observe that the topology is sensitive to the mesh discretization; this is usually not desirable in topology optimization [33]. Further investigation is needed to study the interplay between the neural network and mesh discretization.

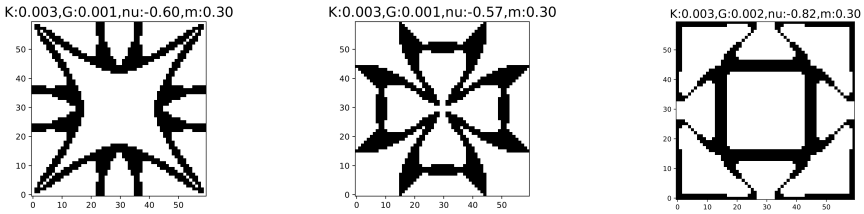

(a) NN: 3×10. (b) NN: 5×20. (c) NN: 6×60. (Redo)

Figure 16: Minimizing Poisson ratio with mass constraint using different NNs.

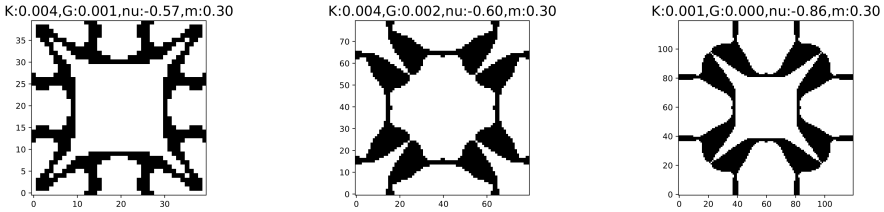

(a) Mesh: 40×40. (b) Mesh: 80×80. (c) Mesh: 120×120.

Figure 17: Minimizing Poisson ratio for different mesh sizes.

A.5 Sampling at Higher Resolution

Once the optimization is completed, the global representation of the density field via the NN allows us to sample the field at a finer resolution and extract a high-resolution topology at no additional cost. This is illustrated in Figures 18 and 19. Observe that we exploit the non-linear NN representation of the density field for resampling, i.e., it is not a simple linear interpolation between pixels. In other words, suppose $d_1 = NN(x_1, y_1)$ and $d_2 = NN(x_2, y_2)$ are the density values at two neighboring pixels. A linear interpolation will yield $0.5(d_1 + d_2)$, whereas the non-linear interpolation yields $NN(0.5(x_1 + x_2), 0.5(y_1 + y_2))$.

(a) Raw output. (b) Sampling at higher resolution.

Figure 18: Sampling the neural network at a higher resolution.

A.6 Evaluation of Poisson Ratio

We consider the negative Poisson's ratio microstructures generated in appendix A.3 and evaluate them using ANSYS [25]. Specifically, the output topology is sampled at a high resolution (in this case 5 times, as seen in Figure 19) and converted to a 2D part using SolidWorks. This is then imported into ANSYS Workbench, where a small axial strain is prescribed and the resultant transverse strain is measured to compute the Poisson's ratio. The results are tabulated in table 3. One can observe that the topology with no single-node connection (fig. 16b) is in good agreement with the results from ANSYS. However, we note that the other two topologies have single-node/hinge connections and, not surprisingly, the homogenized values differ significantly from ANSYS results. Eliminating the single-node/hinge connections is important both for manufacturability and for accurate modeling; this will be explored in the future using, for example, methods described in [23, 42].

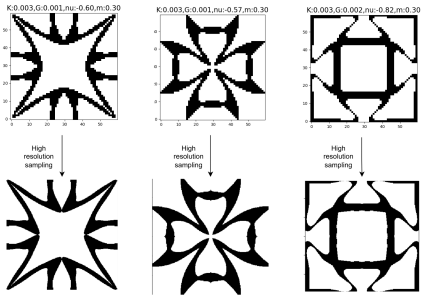

Figure 19: Results of Figure 16 are sampled at $5\times$ resolution ($60 \times 60 \rightarrow 300 \times 300$)

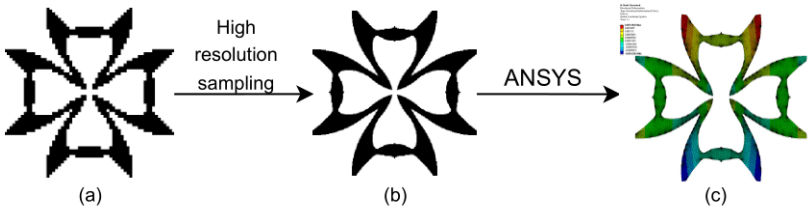

Figure 20: (a) Topology using the default mesh. (b) topology sampled at high resolution. (c) High-resolution geometry imported and analyzed using ANSYS.

A.7 Multiple Materials

Next consider maximization of K, subject to a mass constraint ($\hat{m} = 0.3$), with two, three and four materials. The material properties are summarized in Table 4.

The results are illustrated in Figure 21 (compare against Figure 8a for single material). The final bulk modulus K^* for the three cases are 0.172, 0.225 and 0.240, respectively (compared to 0.091 for single material). Observe that the bulk modulus increases as additional materials are introduced.

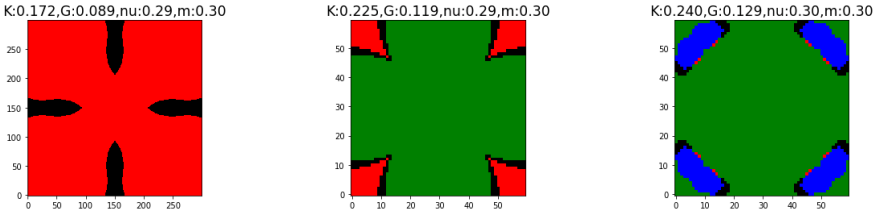

(a) Two materials. (b) Three materials. (c) Four materials.

Figure 21: Maximizing K with mass constraint using multiple materials.

Topology	Homogenized (coarse)	Homogenized (resampled)	ANSYS
fig. 16a	-0.60	-0.65	-1.00
fig. 16b	-0.57	-0.57	-0.60
fig. 16c	-0.82	-0.87	-1.12

Table 3: Evaluation of Poisson's ratio.

Material	Color code	E	ν	λ
0	White	0.001	0.3	0
1	Black	1	0.3	1
2	Red	0.2	0.3	0.2
3	Green	0.3	0.3	0.25
4	Blue	0.4	0.3	0.3

Table 4: Material properties.